Hindawi
Advances in Polymer Technology
Volume 2022, Article ID 4197365, 17 pages
https://doi.org/10.1155/2022/4197365

Research Article

High Flux and Antifouling Nanofiltration Membrane Modified by Ag@UiO-66-NH_2 and Its Application for Biphenol A Removal

Qing-Chun Chen,[1,2,3] **Yu Bang**,[1] **Lu Li**,[1] **and Hui-Yu Deng**[1,2]

[1]*Jiangxi Province Key Laboratory of Polymer Micro/Nano Manufacturing and Devices, East China University of Technology, Nanchang 330013, China*
[2]*State Key Laboratory of Nuclear Resources and Environment, East China University of Technology, Nanchang 330013, China*
[3]*State Key Laboratory of Petroleum Pollution Control, Beijing 102206, China*

Correspondence should be addressed to Hui-Yu Deng; denghuiyu001@163.com

Received 31 August 2021; Revised 20 December 2021; Accepted 23 December 2021; Published 22 January 2022

Academic Editor: Gyorgy Szekely

Owing to the specific porous structure which could provide additional passage channel for some molecules, metal organic frameworks are attractive candidates for enhancing permeability and selectivity of membranes in pervaporation, reverse osmosis, and gas separation. In this experiment, Ag@UiO-66-NH_2 was introduced into polyamide separation layer by interfacial polymerization of triethylenetetramine and 1,3,5-benzenetricarboxylic acid chloride for nanofiltration. The results indicated that Ag@UiO-66-NH_2 nanoparticles did endow the membranes with rapid diffusion pathways for water molecules. When the content of Ag@UiO-66-NH_2 was 0.03 g, the prepared membrane (NF-Ag-3) showed high flux about 47.3 $L{\cdot}m^{-2}{\cdot}h^{-1}$ at 0.6 MPa, which is about 2-fold higher than that of polyamide membrane without Ag@UiO-66-NH_2, while the $MgSO_4$ rejection rate remained about 87.4%. The membrane also showed excellent antifouling properties, and the water flux recovery ratio was 95.6% after filtration BSA solution. When it was applied for 50 mg/L bisphenol A removal, the rejection rate reached 94.6%, and the flux is about 49.1 $L{\cdot}m^{-2}{\cdot}h^{-1}$. Moreover, Ag particles on UiO-66-NH_2 rendered the membrane with good inhibition for *Escherichia coli*. The antibacterial rate of the membranes is above 95% when the loading of Ag@UiO-66-NH_2 is more than 0.03 g.

1. Introduction

Compared with reverse osmosis, nanofiltration shows advantages of low energy consumption and high separation efficiency. Therefore, it has been widely applied in desalination of brackish and seawater, reclamation of waste water from medicine, chemical industry, etc. [1, 2]. However, membrane fouling caused by organic and microbial contamination or inorganic deposition deteriorates the performance of nanofiltration membranes which shortens the membranes service life and increases the application cost [3–9].

In order to improve the antifouling performances of the membranes, hydrophilic polymers as polyvinyl pyrrolidone (PVP) [10], polyethylene glycol (PEG) [11, 12], polyvinyl alcohol (PVA) [13], and zwitterionic polymers [14–18] were introduced into nanofiltration membranes. Due to the hydrogen bonds between these hydrophilic polymers and water, a hydrate layer could form which prevents the protein and other contaminants setting on the membrane, thereby improving solution flux recovery. Deng et al. prepared a nanofiltration membrane with zwitterionic PEI moieties which showed Lys solution flux recovery rate about 91.9% [17]. Commercial membrane NF90 modified by carboxyl betaine methacrylate (PCBMA) containing quaternary ammonium salt showed BSA flux recovery rate near 96.49%, and the inhibition rate to Escherichia coli and Bacillus subtilis was 99% [18].

Besides hydrophilic polymers described above, functional nanoparticles as TiO_2, ZnO, and graphene oxide were also applied to construct antifouling nanofiltration membranes because of their hydrophilic and photocatalytic activities [19–26]. Vatanpour et al. [19] prepared a composite nanofiltration membrane by blending TiO_2@multiwalled carbon nanotubes with polyethersulfone (PES). Pure water

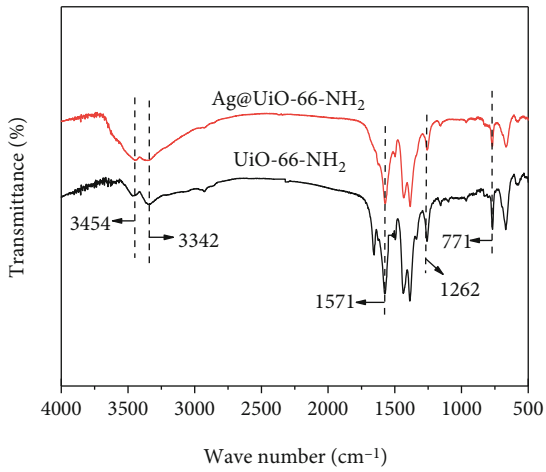

Figure 1: FTIR spectra of UiO-66-NH_2 and Ag@UiO-66-NH_2.

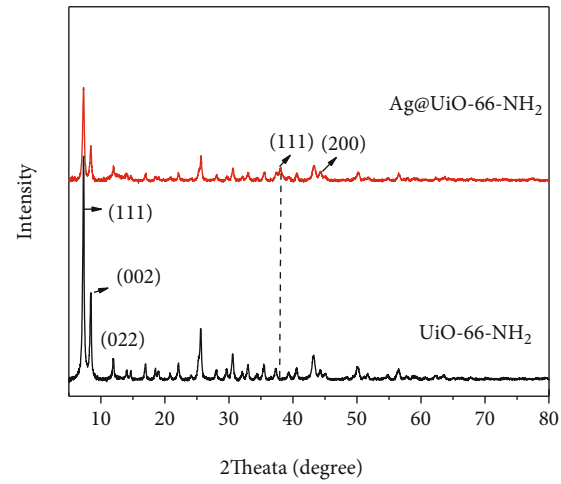

Figure 2: XRD patterns of UiO-66-NH_2 and Ag@UiO-66-NH_2.

flux of the blend membranes increased with the content of TiO_2@MWCNTs. The reversible fouling value of the membrane containing 0.1 wt% TiO_2@MWCNTs remarkably reduced from 46.9% (bare PES membrane) to 17.0%. This is attributed to the smoother surface and synergistic photocatalytic activity of nanoparticles. Soria et al. [20] studied the effects of ZnO/TiO_2 mixing catalysts on PDA-modified membranes. In comparison with pristine membrane, 125% increase in the hydrophilicity of the modified membranes was evidence. Meanwhile, Zn^{2+} released from ZnO nanoparticles can destroy DNA and cytoplasm of bacteria; therefore, the membranes showed excellent antimicrobial activity.

Recently, metal organic framework has attracted a lot of attention because its specific porous structure could enhance the permeability and selectivity of the membrane [27–32]. Performances of the nanofiltration membrane can be adjusted by introducing the MOFs into the separation layer or to the substrate membrane. A composite membrane prepared by spin coating of But-8(A)/PET on the hydrolyzed polyacrylonitrile substrate membrane exhibited high water permeance of 683 $L \cdot m^{-2} \cdot h^{-1} \cdot MPa^{-1}$ (But-8(A) = $Cr_3(\mu_3\text{-}O)(H_2O)_3(NDC(SO_3H_5/_6)_2)_3$) [27]. Midsan et al. [28] prepared a hydrophilic polyamide membrane on a polysulfone substrate membrane modified by copper benzene-1,3,5-tricarboxylate (CuBTC) nanoparticles. Water contact angle of the membrane decreased from 70.25° to 59.02° which was attributed to the MOFs promoting formation of more linear structure of poly(piperazineamide) entangled with –COOH pendant groups. Moreover, a notable increment of rejection against NaCl could be attained by increasing the CuBTC content in the substrate membrane.

Typically, Ag-based and Cu-based materials show broad spectrum of antimicrobial activity; therefore, MOFs containing Ag or Cu element were applied to further improve antifouling performance of the membranes; however, it remains in its infancy. Fatemeh Seyedpour et al. [30] developed a novel antifouling TFC polyamide membrane by surface anchoring Ag^+ via in situ assembly of Ag-MOFs which imparted highly potent antibacterial property to the membrane. Similar works were reported by Pejman et al. [31, 32].

However, the silver element in Ag-MOFs described above [30–32] is ionic state. Compared with Ag^+, Ag nanoparticles have better long-term bacteriostasis [33–35]. Its bacteriostatic property combines the effects of silver element and nanomaterials. In solution, it generates Ag^+ which destroy the protein cell membrane by replacing Mg^{2+} and Ca^{2+} in the cell membrane and induce the cell die. Meanwhile, due to the large specific surface area and high surface activity of nanoparticles, it catalyzes formation of reactive oxygen radicals which destroy the nucleic acid and DNA of bacteria and inhibit the reproduction of bacteria. Herein, Ag nanoparticles [36], Ag/TiO_2 [37], and Fe_3O_4@Cs@Ag composite [38] were applied to improve antibacterial performance of microfiltration and ultrafiltration membranes.

Inspired by the works above, Ag nanoparticle deposited UiO-66-NH_2 (Ag@UiO-66-NH_2) was applied to modify polyamide nanofiltration membrane in this experiment. UiO-66-NH_2 is a metal–organic framework materials with high heat resistance, water stability, and corrosion resistance. Owing to the large specific area, high porosity, and the chelation of N atom and transition metal ions, UiO-66-NH_2 and its derivatives have been widely used as adsorbent for transition metal ions [39]. Recently, some researchers focused on the applications of UiO-66-NH_2 in membrane separation. Xu et al. found hydrophilic -NH_2 groups in UiO-66-NH_2 can facilitate water transport. Compared with UiO-66-F4 and UiO-66, the mixed matrix membranes composed of UiO-66-NH_2 and 6FDA-HAB/DABA polyimide have superior separation performance in dehydration of C1-C3 alcohols via pervaporation [40].

A polyamide thin film nanocomposite (TFN) membrane incorporated defect-engineered UiO-66-NH_2 [41] showed enhancements of the permeability and selectivity to Na_2SO_4 solution simultaneously. Polymer was applied to bridge the gap between UiO-66-NH_2 and the membrane matrix, so as to decrease the defect in mixed-matrix membrane. The performances of the membrane were improved obviously [42–44]. However, to our knowledge, the works on modification of nanofiltration membrane by Ag@UiO-66-NH_2 were not reported before.

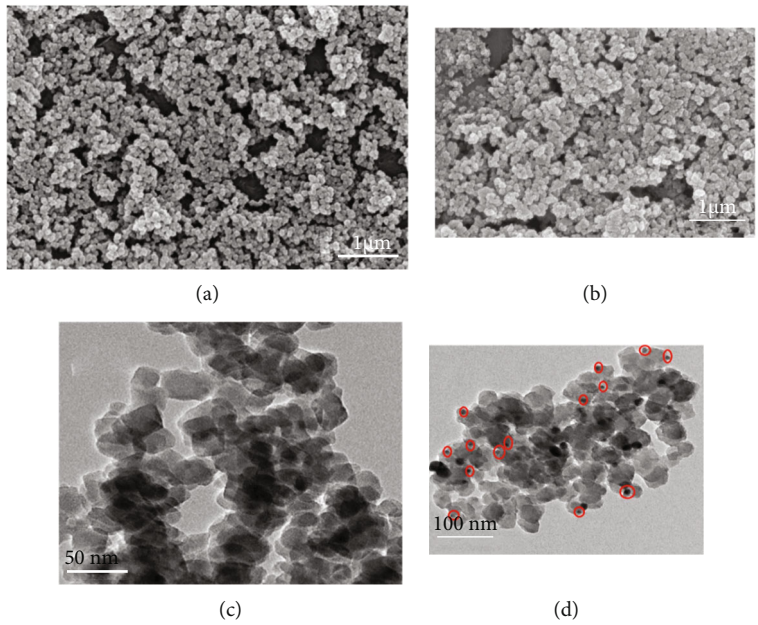

Figure 3: (a) and (c) are SEM and TEM images of UiO-66-NH_2;(b) and (d) are SEM and TEM images of Ag@UiO-66-NH_2.

In this work, Ag@UiO-66-NH_2 was incorporated into the polyamide layer by interfacial polymerization of triethylenetetramine and 1,3,5-benzenetricarboxylic acid chloride. The effects of Ag@UiO-66-NH_2 on membrane structure and performances were investigated. The antifouling performances for BSA and Lys and antimicrobial properties to *Escherichia coli* were evaluated. The membrane prepared at optimized condition was applied for bisphenol A removal. The concentration and pH value of BPA solution, operating pressure on bisphenol A rejection rate and flux were elucidated.

2. Results and Discussion

2.1. Characterization of Ag@UiO-66-NH_2. Infrared spectra of UiO-66-NH_2 and Ag@UiO-66-NH_2 are shown in Figure 1. The typical absorption peaks of UiO-66-NH_2 changed insignificantly after deposition of Ag particles. The peaks at 3454 cm^{-1} and 3342 cm^{-1} attribute to asymmetric and symmetric stretching vibration of N-H in UiO-66-NH_2 and Ag@UiO-66-NH_2 and stretching vibration of O-H in UiO-66-NH_2, Ag@UiO-66-NH_2, and adsorption water. The peaks at 1571 cm^{-1}, 1262 cm^{-1}, and 771 cm^{-1} correspond to bending vibration of N-H, stretching vibration of C-N in aromatic amine, and C-C bending vibration in benzene ring, respectively.

XRD spectra of UiO-66-NH_2 and Ag@UiO-66-NH_2 are shown in Figure 2. The diffraction peaks of 2θ at 7.4°, 8.5°, and 12.0° are assigned to (111), (002), and (022) planes of UiO-66-NH_2 crystal [45]. Compared with UiO-66-NH_2, a new diffraction peak appeared at 37.9°, and the intensity of the peak at 44.2°increased in the spectrum of Ag@UiO-66-NH_2, which is attributed to the diffraction peaks of (111) (JCPDSNo.87-0720) and (200) crystal planes of Ag particles. This is in agreement with the result of Ref. [38].

SEM and TEM images (Figures 3(a) and 3(c)) indicate the prepared UiO-66-NH_2 is octahedral structure, and the particle size is about 40 nm. After deposition of Ag nanoparticles, morphology of the UiO-66-NH_2 changed little (Figure 3(b)). However, TEM image demonstrated that there are 5 to 15 nm nanoparticles setting on UiO-66-NH_2 particles (circled by red ring in Figure 3(d)).

EDS analysis identified that these particles contain Ag element (Figure 4). In the EDS spectrum of UiO-66-NH_2, peaks corresponded to the elements of C, N, O, and Zr appeared at 0.277, 0.392, 0.525, and 2.042, respectively. In comparison, peaks corresponded to Ag element appeared at 2.984 in the EDS spectrum of Ag@UiO-66-NH_2 (Figure 4(b)), which further confirmed that Ag particles had been successfully deposited on UiO-66-NH_2.

The nitrogen adsorption/desorption isotherms of UiO-66-NH_2 and Ag@UiO-66-NH_2 at 77 K combine the characteristics of typical I and IV isotherms (Figure 5). The isotherm revealed slightly sharp uptake at relatively low pressure which due to the existence of intrinsic micropores in the sample. The hysteresis loop demonstrated UiO-66-NH_2 and Ag@UiO-66-NH_2 also contain some mesoporous pores. Specific surface area of UiO-66-NH_2 is 421.1 m^2/g, while that of Ag@UiO-66-NH_2 is 533.7 m^2/g. The increased specific area may attribute to the deposition of Ag which provide additional external surface. It should be pointed out that Ag particles may seal some pores on UiO-66-NH_2, so the mean pore of UiO-66-NH_2 decreased from 11.96 nm to 6.69 nm after the deposition of Ag.

2.2. Characterization of Ag@UiO-66-NH_2/PA Nanofiltration Membrane. The chemical composition of PAN substrate membrane and typical NF membranes was characterized by FTIR, and the spectra are shown in Figure 6. In the spectra of PAN membrane, the peaks at 2241 cm^{-1} and 1445 cm^{-1} are the typical stretching vibration of -CN and-CH_2. The

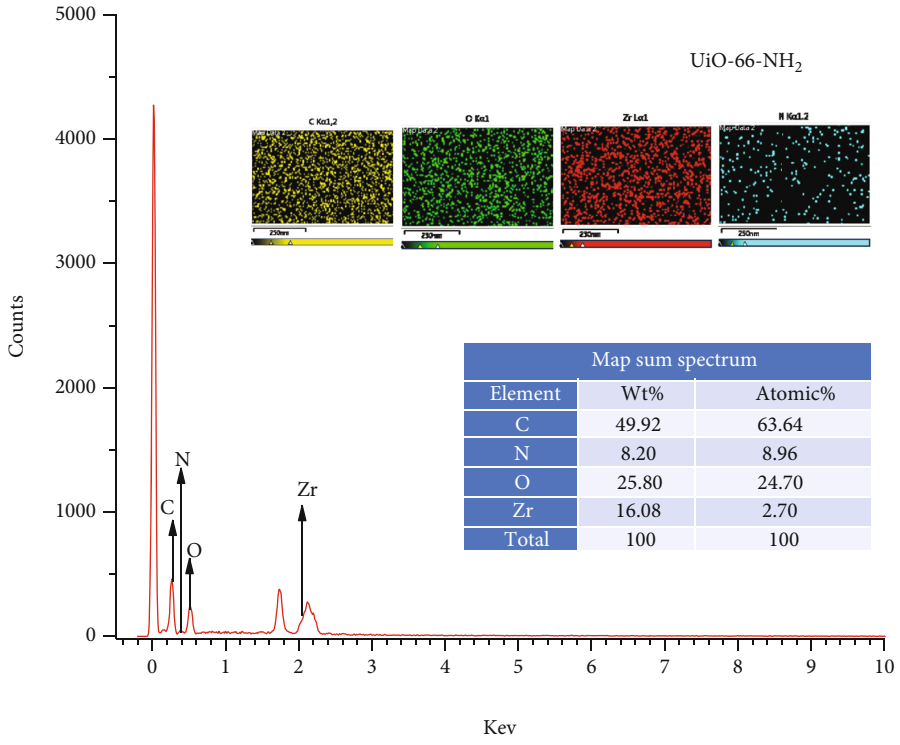

(a)

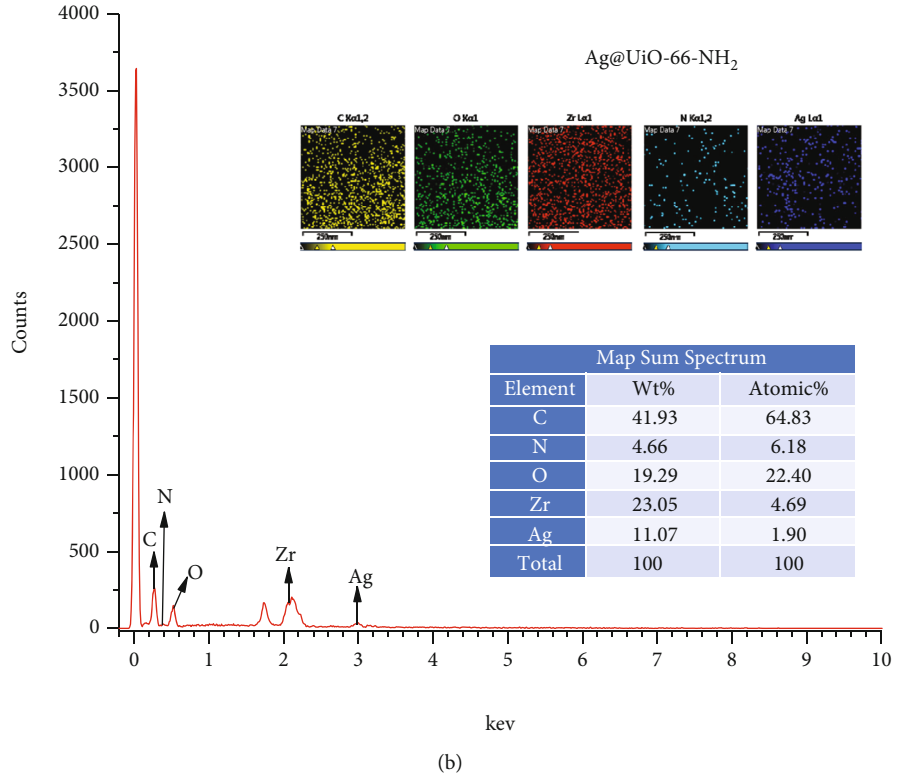

(b)

Figure 4: EDS mapping of (a) UiO-66-NH_2 and (b) Ag@UiO-66-NH_2.

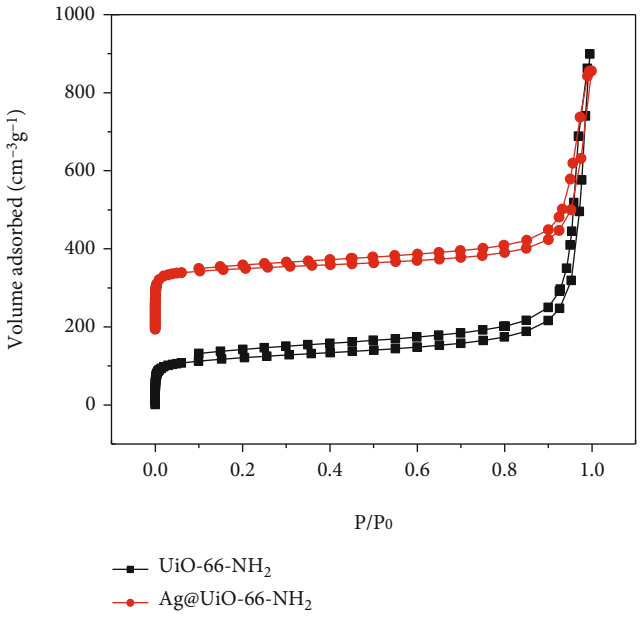

FIGURE 5: The N_2 adsorption/desorption isotherms of UiO-66-NH_2 and Ag@UiO-66-NH_2.

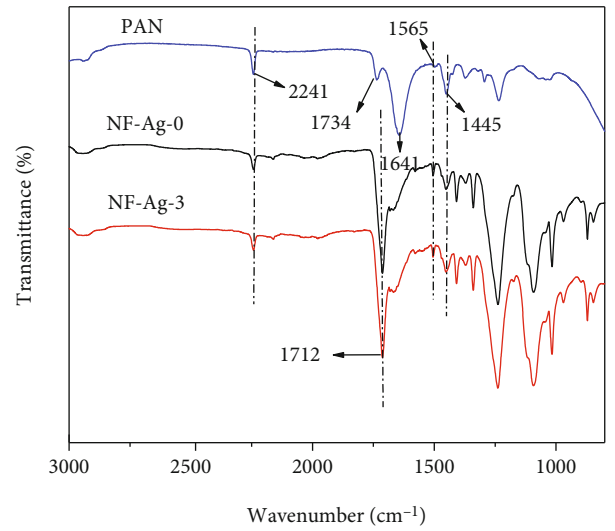

FIGURE 6: FTIR-ATR spectra of typical membranes.

PAN substrate membrane is preserved in deionized water before use, and due to hydrolysis of polyacrylonitrile, there are typical amide absorption peaks appeared in 1565 cm^{-1} corresponds to the bending vibration of amide II, while 1734 cm^{-1} is the characteristic peak of the stretching vibration of ester carbonyl in polyester nonwoven fabric substrate of PAN membrane. In comparison with PAN substrate membrane, the strength of peak at 1565 cm^{-1} of NF-Ag-0 and NF-Ag-3 membrane increased, which attributed to polyamide generated by interfacial polymerization of triethylenetetramine and benzoyl chloride on PAN substrate membrane. The strong absorption peak at 1712 cm^{-1} belongs to carboxy carbonyl generated from the hydration of unreacted acyl chloride of TMC, which overlapped with the ester carbonyl of polyester nonwoven fabric of the substrate membrane.

The surface morphology of PAN substrate membrane and some typical NF membranes is shown in Figure 7. The surface of PAN substrate membrane (Figure 7(a)) was relatively smooth, while the NF membranes were relatively rough. There appeared granular substances on the membrane surface because of the formation of polyamide (Figure 7(b)). After incorporation of Ag@UiO-66-NH_2, the membrane surface became rougher and more larger particles appeared which could enhance the permeability of the membrane in a certain range. It should be pointed out that when the content of Ag@UiO-66-NH_2 was 0.05 g, some particles aggregated together (Figure 7(d)), which deteriorated the membrane performance we will demonstrate in the following section.

Energy spectrum analysis (Figure 8) showed the particles on NF-Ag-3 membrane surface contain elements of C, N, O, Zr, and Ag, and the weight percentage of these elements is 35.38 wt%, 4.99 wt%, 22.58 wt%, 29.69 wt%, and 7.36 wt%, respectively, which confirmed that Ag@UiO-66-NH_2 had been successfully incorporated into the separation layer. Incorporation of Ag@UiO-66-NH_2 to the separation layer plays very important effect on the performance of the membranes, which we will discuss below.

2.3. Separation Performance of Ag@UiO-66-NH_2/Polyamide Membrane. Figure 9 shows the separation performance of Ag@UiO-66-NH_2/polyamide membranes. The salt rejection order for NaCl, $MgCl_2$, Na_2SO_4, and $MgSO_4$ changed from $MgSO_4 \geq Na_2SO_4 > MgCl_2 > NaCl$ to $MgSO_4 > MgCl_2 > Na_2SO_4 > NaCl$ by increasing the content of Ag@UiO-66-NH_2. Compared with pure polyamide membranes, the NaCl retention rate decreased, while that of magnesium salts nearly kept stable (Figure 9(a)).

Meanwhile, the flux of Ag@UiO-66-NH_2/polyamide membranes were larger than that of NF-Ag-0 (without Ag@UiO-66-NH_2) (15.9 L $m^{-2}{\cdot}h^{-1}$). When the loading of Ag@UiO-66-NH_2 was 0.02 g and 0.03 g, the flux increased to 41.3 and 47.3 L $m^{-2}{\cdot}h^{-1}$ for $MgSO_4$ solution, respectively. Further increasing the content of Ag@UiO-66-NH_2, the flux decreased. However, it should be noted that the flux was still lager than that of NF-Ag-0 (Figure 9(b)).

Separation mechanism of NF membranes mainly depends on charge repulsion and size exclusion effect. On one hand, the introduction of Ag@UiO-66-NH_2 impeded the interfacial polymerization and induced a looser membrane structure, which reduce the salt rejection and increase the solution flux. On the other hand, the amount of -NH_2 increased by increasing the loading of Ag@UiO-66-NH_2. The protonation of -NH_2 groups may increase the effective positive charge of the membrane which would promote the electrostatic repulsion between membrane and the multivalent cations as Mg^{2+}. Moreover, the hydrated radius of Mg^{2+} (0.300 nm) is larger than that of Na^+ (0.178 nm) [41]; therefore, the rejection rate of Mg^{2+} salts nearly kept stable while that of the Na^+ salts decreased with incorporation of Ag@UiO-66-NH_2.

In addition, the membrane flux was also enhanced by the following factors: (1) The porous structure of Ag@UiO-66-NH_2 provided additional passage channel for water

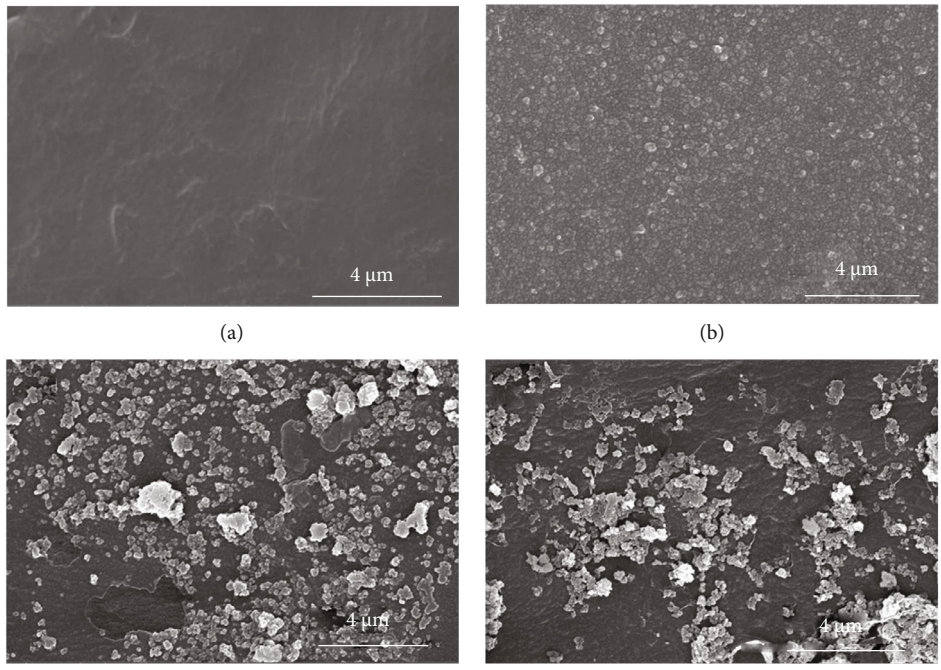

Figure 7: SEM images of typical membranes. (a) PAN substrate membrane, (b) NF-Ag-0, (c) NF-Ag-3, and (d) NF-Ag-5.

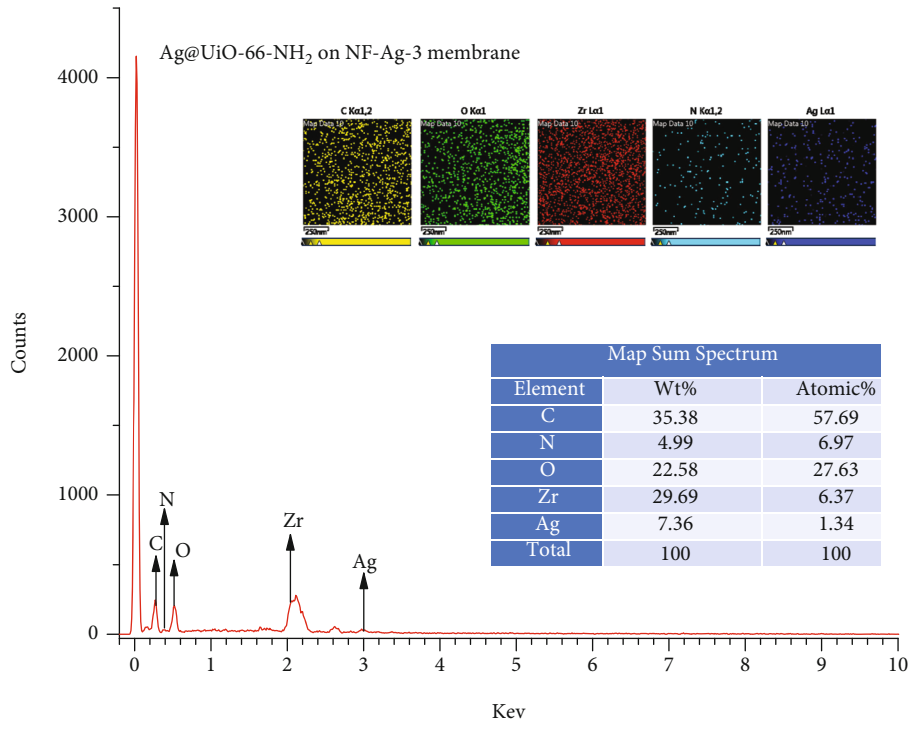

Figure 8: EDS mapping of Ag@UiO-66-NH_2 on NF-Ag-3 membrane.

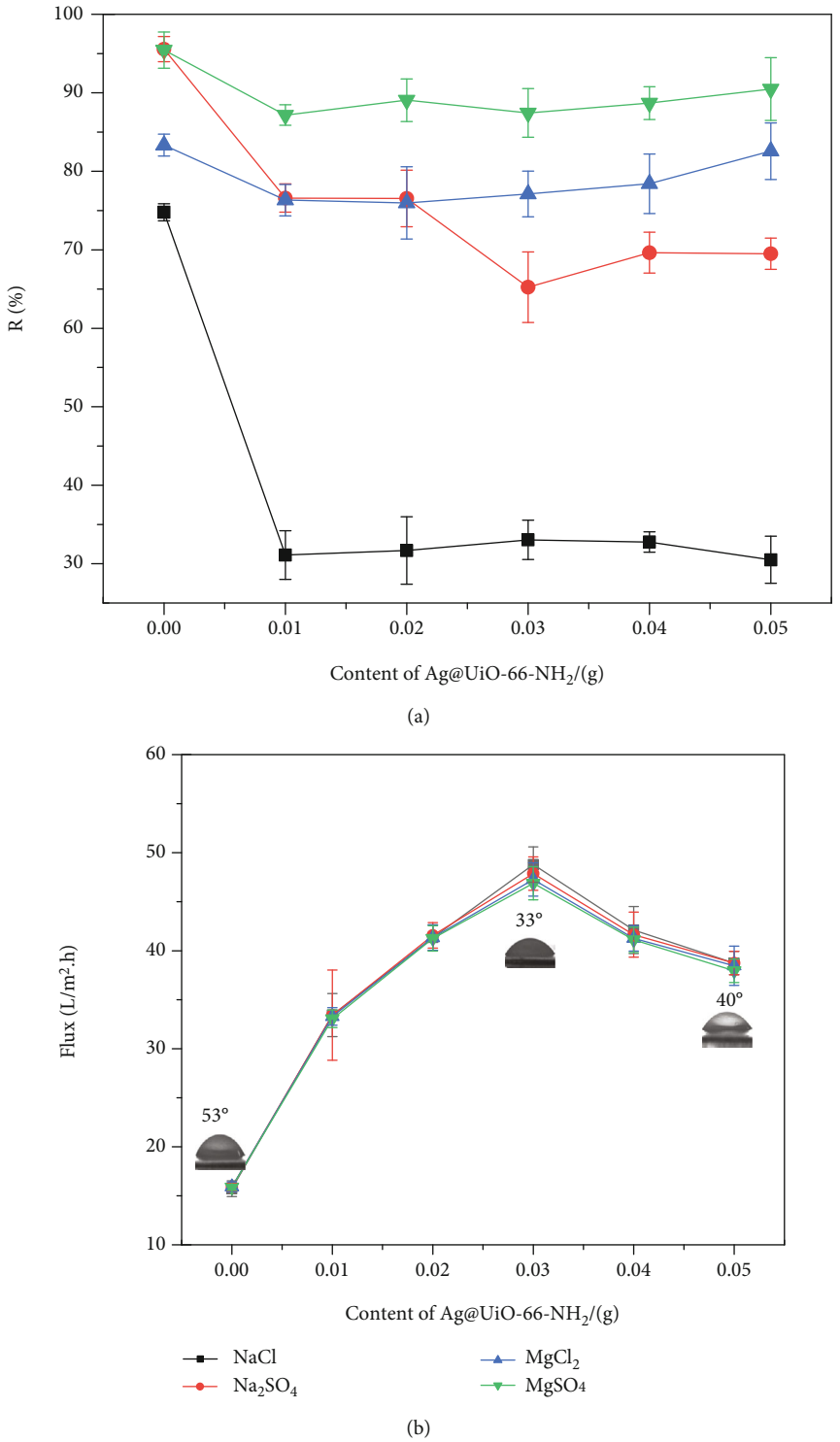

Figure 9: Separation performance of Ag@UiO-66-NH_2 membrane. (a) Rejection. (b) Flux.

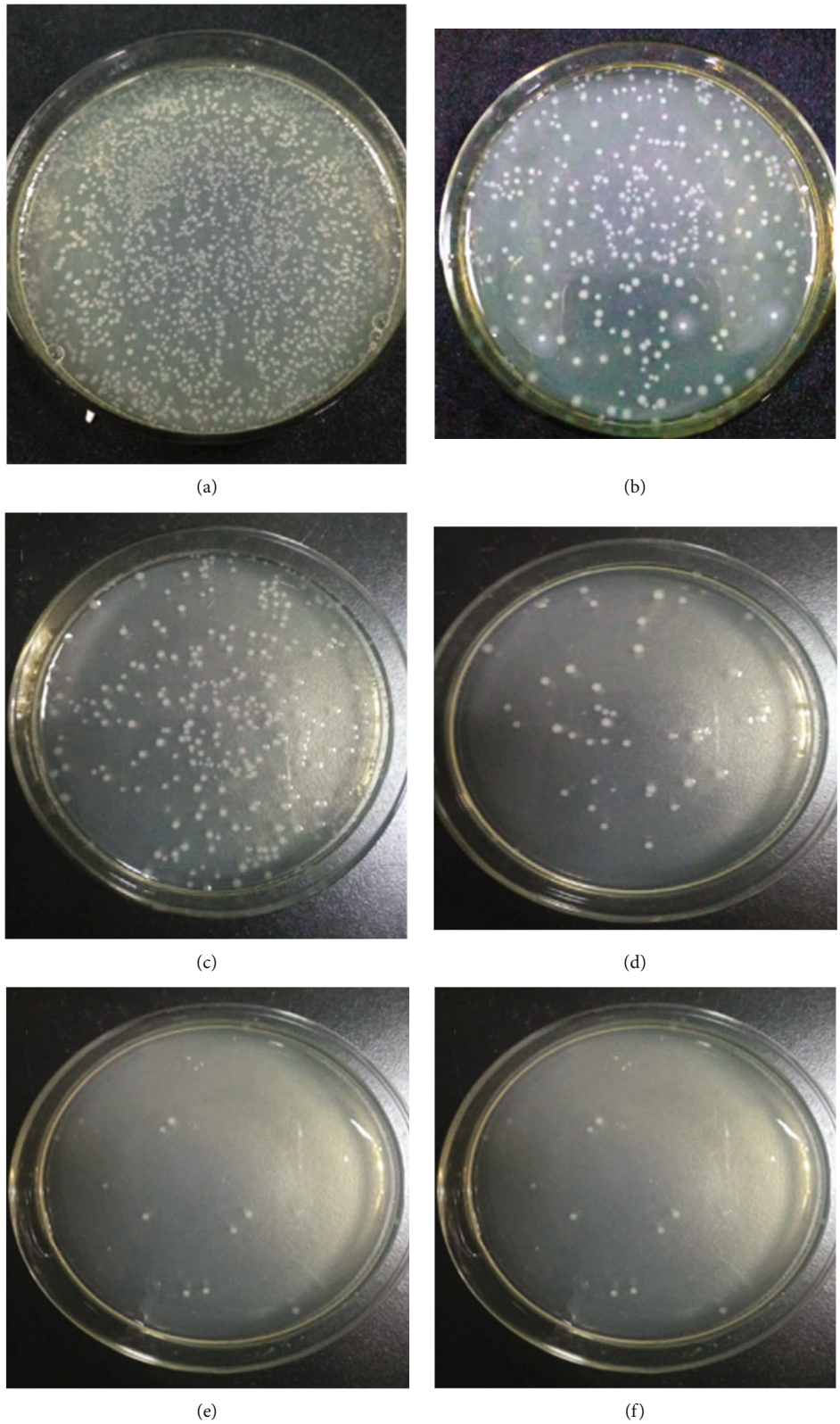

(a) (b) (c) (d) (e) (f)

Figure 10: Continued.

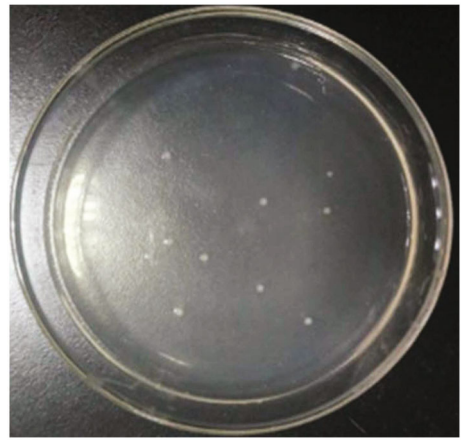

(g)

Figure 10: Antibiosis performances of membrane. (a) PAN substrate membrane, (b) NF-Ag-0, (c) NF-Ag-1, (d) NF-Ag-2, (e) NF-Ag-3, (f) NF-Ag-4, and (g) NF-Ag-5.

molecules. (2) The hydrogen bonds between -NH_2 groups on Ag@UiO-66-NH_2 and triethylenetetramine (TETA) could slow down the diffusion rate of the TETA to oil phase, which is beneficial to fabricate a thinner separation layer and reduce the water transfer resistance. (3) The hydrophilicity of the membranes was improved by incorporation of Ag@UiO-66-NH_2. For instance, the water contact angle of pure polyamide membrane was 53°, while that of NF-Ag-3 was only 33°.

It should be pointed out that some pores may be partly sealed by aggregated Ag@UiO-66-NH_2 particles (Figure 7(d)) when further increasing the loading of Ag@UiO-66-NH_2 to 0.04 g and 0.05 g, so compared with NF-Ag-3, the flux decreased.

2.4. Antibiosis Performances of Ag@UiO-66-NH_2/PA Nanofiltration Membranes. Silver nanoparticles can destroy the phospholipid bilayer and permeability of cell membrane and cause sugar and protein leaking from the bacteria cell. Hence, induced cells die. Furthermore, the high surface activity of the particles also leads the bacterial to die [33–35]. The antibacterial performance of Ag@UiO-66-NH_2/PA nanofiltration membranes to E. coli was investigated (Figure 10). The results showed that the antibacterial ability of the membranes was enhanced by incorporating Ag@UiO-66-NH_2. The higher the Ag@UiO-66-NH_2 content, the better the antibacterial was. The antimicrobial rate of NF-Ag-0 was 35.2% (Figure 10(b)). After adding 0.03 g Ag@UiO-66-NH_2, the antimicrobial rate of the membrane increased to 97% (Figure 10(e)). Further increasing the content to 0.05 g, the antimicrobial rate nearly reached 100% (Figure 10(g)).

2.5. Antiprotein Adsorption of Ag@UiO-66-NH_2/PA Nanofiltration Membrane. The antiprotein adsorption performance of the optimal membrane NF-Ag-3 and its application for bisphenol A removal were evaluated. BSA and Lys were applied as the model proteins.

After filtration of BSA solution for the first cycle, flux recovery rate (FRR), irreversible pollution (R_{ir}), and reversible pollution (R_r) of NF-Ag-3 were 95.6%, 4.4%, and 3.6%. After filtration for three cycles, FRR, R_{ir}, and R_r of NF-Ag-3 slightly changed to 89.4%, 10.6%, and 3.6% (Figure 11(a)). In comparison, those of NF-Ag-0 were 88.4%, 11.6%, and 5.2% for the first cycle, and after running for three cycles, those were changed to 70.4%, 29.6%, and 4.7%, respectively.

NF-Ag-3 membrane also showed excellent anti-Lys adsorption performance. As shown in Figure 11(b), FRR, R_{ir}, and R_r of NF-Ag-3 membrane were 87.5%, 12.5%, and 2.7%, respectively, for separation Lys solution for three cycles, while those of NF-Ag-0 were 67.2%, 32.8%, and 3.7%.

These attributed to the hydrophilicity of NF membrane was improved by Ag@UiO-66-NH_2. Water contact angle of NF-Ag-0 was 53°, while that of NF-Ag-3 decreased to 33°. In the filtration process, ordered water layer formed on the membrane surface through hydrogen bonding, which not only reduces the nonspecific binding between proteins and the membrane surface but also reduces the electrostatic force between proteins and the membrane surface, thereby reducing the protein adsorption on the membrane surface.

2.6. Application of Ag@UiO-66-NH_2/PA Nanofiltration Membrane for Bisphenol A Removal. Bisphenol A is a kind of typical environmental endocrine disruptors (EDCs), which has certain embryotoxicity and teratogenicity, and can increase the risk of ovarian cancer, prostate cancer, asthma, and leukemia. BPA in water is difficult to be biodegraded and has strong resistance to chemical oxidation. In this experiment, the optimal NF membrane NF-Ag-3 membrane was applied for bisphenol A removal, and the effects of concentration, operation pressure, and pH value on bisphenol A removal were explored.

As shown in Figure 12, the rejection rate for 5 mg/L bisphenol A solution was nearly 100% at 0.6 MPa. Concentration polarization effect on the performance of the membrane is insignificant when the bisphenol A concentration ranged from 5 mg/L to 50 mg/L. The rejection rate of 50 mg/L bisphenol A only slightly reduced to 94.6%, while

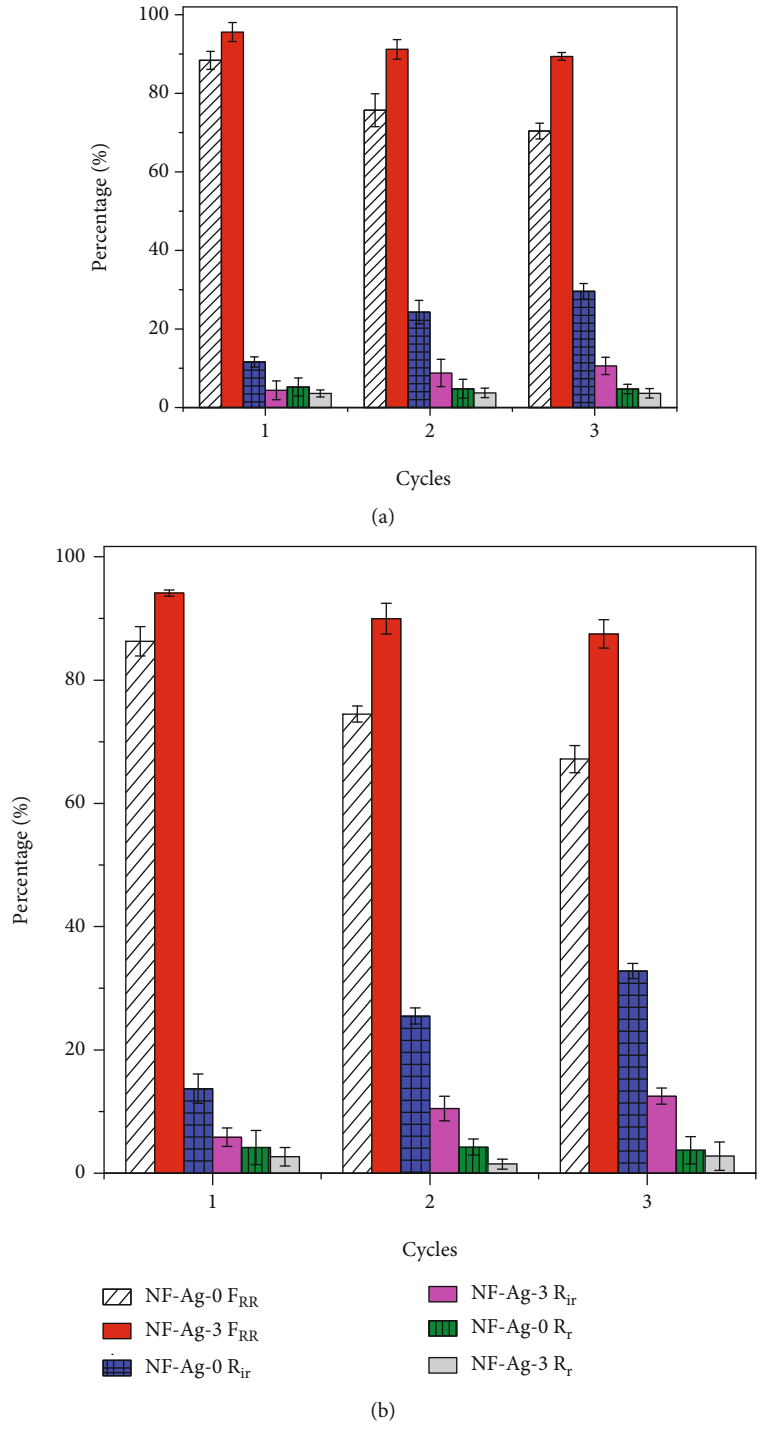

Figure 11: Antiprotein adsorption with NF-Ag-3 membrane. (a) BSA; (b) Lys.

the flux remained stable about 49.1 $L \cdot m^{-2} \cdot h^{-1}$ at 0.6 MPa (Figure 12(a)).

Figure 12(b) indicated that the flux increased with increasing operation pressure, the solution flux to operation pressure ratio of NF-Ag-3 is about 61.6 $L \cdot m^{-2} \cdot h^{-1} \cdot MPa^{-1}$, and the bisphenol A rejection rate is very stable; the removal rate only slightly decreased from 94.6% to 92.5% when operation pressure changed from 0.6 MPa to 0.8 MPa.

When the pH value of BPA solution (50 mg/L) was adjusted from 4 to 10, the flux was remained above 45 $L \cdot m^{-2} \cdot h^{-1}$; however, rejection rate decreased from 94.6% to 85.6%, which may attribute to the dissociation of bisphenol A. Dissociation constant pKa of bisphenol A is 9.8, and when pH value was adjusted to 10, bisphenol A is easier to dissociate into negatively charged ions, which attracts the positive charge on the membrane surface and increases the

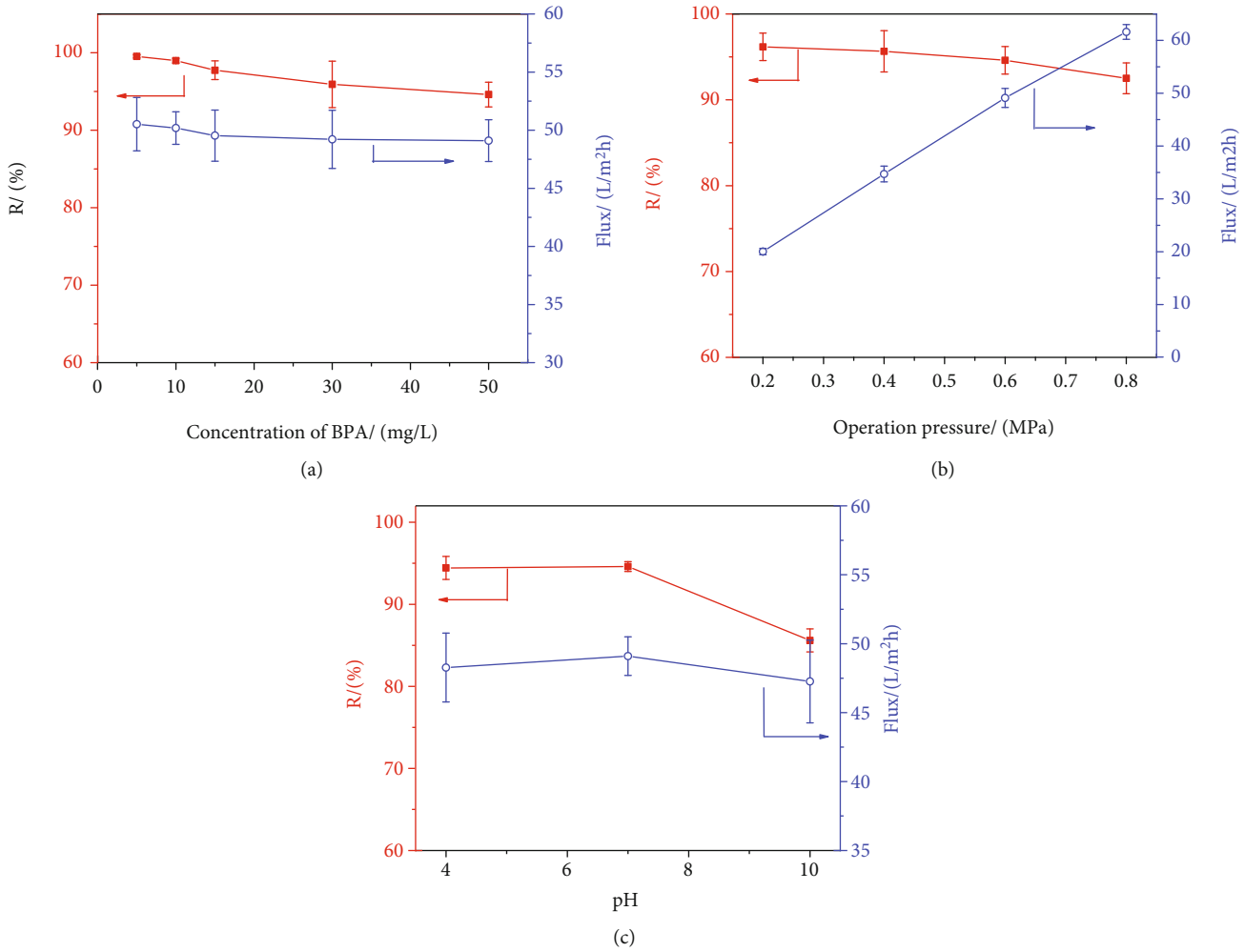

Figure 12: Application of NF-Ag-3 on removing BPA. (a) Concentration, (b) operating pressure, and (c) pH value.

concentration of bisphenol A ions near the membrane surface which promotes the permeation of bisphenol A, thus reducing the removal rate of bisphenol A. Therefore, it is appropriate be used in solution with pH less than 9.8.

Compared with other membranes reported in the literature (Table 1), the permeability and BPA rejection rate of this work is well. According to the reported literature [46–52], the mechanism for BPA removal by membrane is mainly chemical (hydrogen bonding), and physical (hydrophobic interactions) adsorptions occur in the membrane filtration process, size exclusion, catalysis, etc. In this work, considering the results as follows: (1) the rejection rate of BPA is more than that of the salts; (2) the membrane is hydrophilic, we speculate that the mechanism for BPA removal of Ag@UiO-66-NH_2/PA membrane is mainly attributed to size exclusion. Adsorption may contribute little to the BPA removal. This will be verified by further experiments, and we will report it later.

3. Conclusions

The fabrication of a high flux and antifouling Ag@UiO-66-NH_2/polyamide nanofiltration membrane and its application for biphenol A removal were demonstrated in this work. Ag@UiO-66-NH_2 was first prepared by solvothermal process; then it was successfully introduced into the polyamide separation layer via interfacial polymerization. Morphology, hydrophilicity, and salt rejection order of the membranes changed with the content of Ag@UiO-66-NH_2. The solution flux increased obviously by the introduction of Ag@UiO-66-NH_2. Depending on charge repulsion and size exclusion effect, the optimal membrane NF-Ag-3 showed salt rejection order as $MgSO_4$>$MgCl_2$>Na_2SO_4>NaCl. Salt rejection rate for 1000 mg/L $MgSO_4$ solution of NF-Ag-3 membrane was 87.4%, and the flux reached 78.8 L·m^{-2}·h^{-1}·MPa, which was 2-fold higher than that of membrane without Ag-MOFs. Furthermore, hydrophilic nature of NF-Ag-3 and antimicrobial property of Ag nanoparticles endow the membrane with excellent antifouling and antimicrobial performance; the antimicrobial rate of the membrane is above 95% which renders the membrane maintain original performances in long-time running.

When it was applied for BPA removal, the rejection rate of 50 mg/L BPA reached 94.6% and the flux was about 81.8 L/m^2·h·MPa, which is superior to most membranes reported in literature. Hence, NF-Ag-3 membrane has

Table 1: Comparison of solution permeability and BPA rejection of various membranes.

Membrane	Rejection (%)	Flux (L/m^2·h·Mpa)	Testing condition		Ref.
			C_{BPA}	Pressure (MPa)	
LBL-PI (NF)	92.1	178	34.2 mg/L	0.2	[46]
Ag@UiO-66-NH_2/PA	94.6	81.8	50 mg/L	0.6	This work
AD SWRO	97	8.5	50 mg/L	1	[47]
CE BWRO	15	24.1	50 mg/L	1	[47]
XLE BWRO	95	59.1	50 mg/L	1	[47]
NF270	80	148.6	50 mg/L	1	[47]
NF90	92	60.5	50 mg/L	1	[47]
BW30	92	19.7	50 mg/L	1	[47]
NFD	83	17.97	300 mg/L	0.6	[48]
NF90	93	25.23	300 mg/L	0.6	[48]
NF270	83	24.55	300 mg/L	0.6	[48]
CK	93	2.34	300 mg/L	0.6	[48]
ESNA	96	22.68	300 mg/L	0.6	[48]
NF90	90	38.4	750 μg/L	1.3	[49]
NF270	40	54.0	750 μg/L	1.3	[49]
PES-PEGHBS	35	~110.8 (pure water)	500 mg/L	0.55	[50]
	60	—	100 mg/L		[50]
	75	—	50 mg/L		[50]
	72	—	5 mg/L		[50]
TS 80	70.7	50	2 μg/L	1.7	[51]
RO X20	95.3	33	2 μg/L	1.7	[51]
PVDF	27[a], 9[b]	7100	5 mg/L	0.1	[52]
PVDF-PVP	100[a], 20[b]	3550	5 mg/L	0.1	[52]
PVDF-a-carbon	24[a], 2[b]	5107.8	5 mg/L	0.1	[52]
PVDF-MnO_2	54[a], 41[b]	4128.7	5 mg/L	0.1	[52]
PVDF-Ac	100[a], 9[b]	4652.8	5 mg/L	0.1	[52]
PVDF-PVP-MnO_2	100[a], 20[b]	3784.6	5 mg/L	0.1	[52]
XLE	83	—	100 μg/L	0.5	[49]

[a]Initial rejection rate; [b]rejection rate after 30 min.

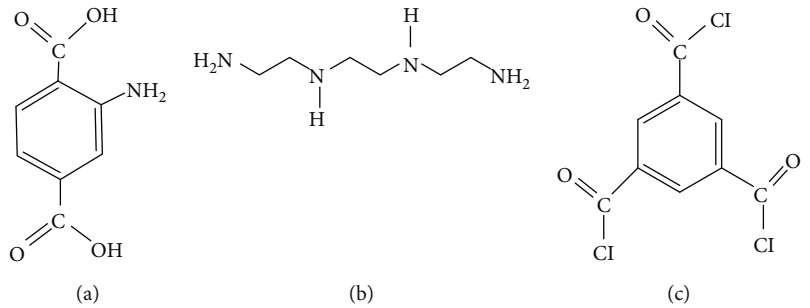

(a) (b) (c)

Figure 13: Schemes of (a) 2-amino-terephthalic acid, (b) triethylenetetramine, and (c) 1,3,5-benzenetricarboxylic acid chloride.

potential application in BPA removal. The application performances of the membrane in nature conditions and the BPA removal mechanism are under working; the results will be reported later. It should be noted that the preparation of Ag@UiO-66-NH_2 is time-consuming which will impede the membrane's industrial application. Thereby, how to improve the production efficiency needs further investigating.

4. Experimental Section

4.1. Materials and Reagents. Polyacrylonitrile (PAN) ultrafiltration membrane (molecular weight cutoff = 50000) was purchased from Shanghai Lanjing Membrane Technology Co., Ltd. Zirconium tetrachloride ($ZrCl_4$), 2-amino-terephthalic acid (NH_2-BDC), triethylenetetramine (TETA),

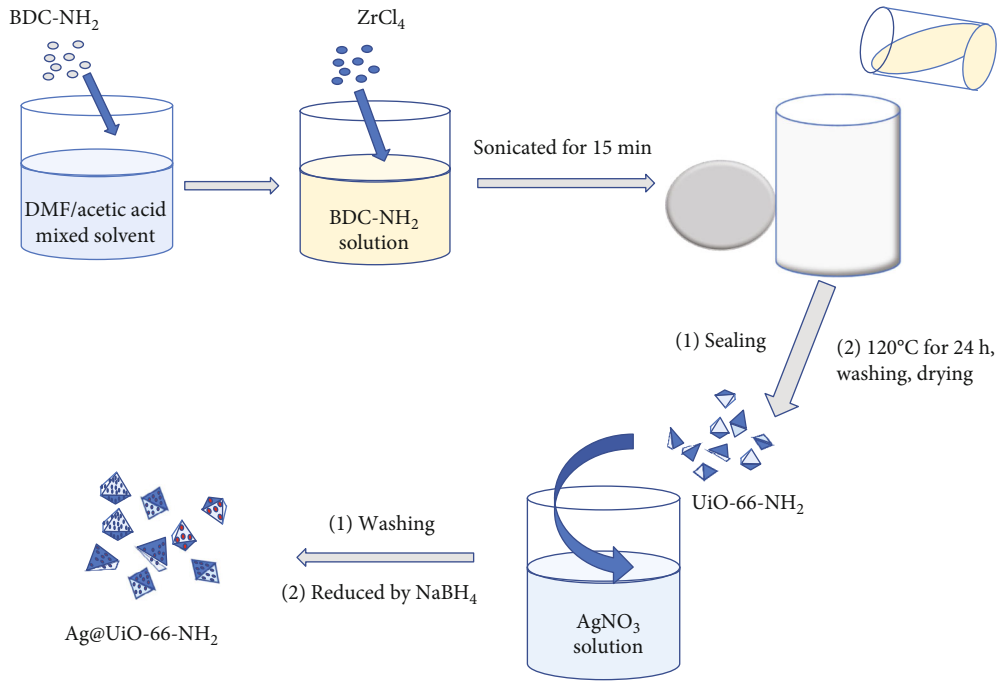

Figure 14: Schematical illustration of the preparation of Ag@UiO-66-NH_2.

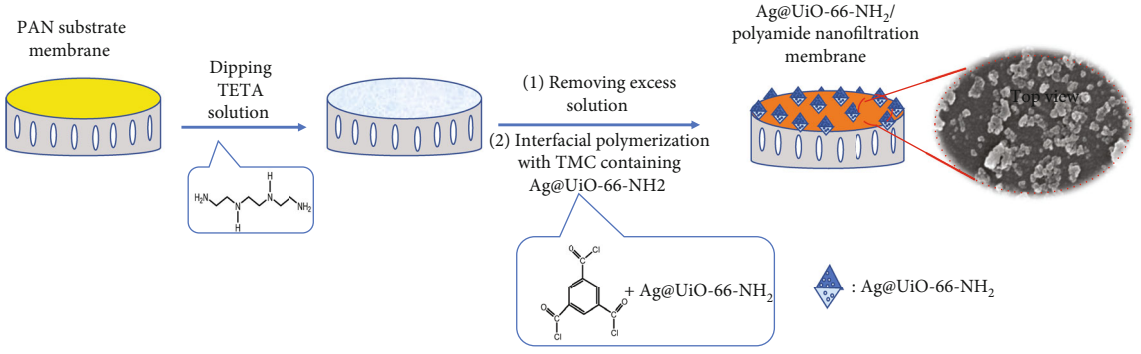

Figure 15: Fabrication of Ag@UiO-66-NH_2/polyamide nanofiltration membrane.

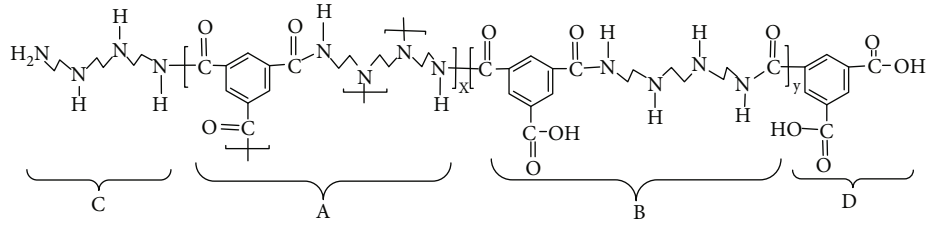

Figure 16: Possible polymerization reaction between triethylenetetramine and 1,3,5-benzenetricarboxylic acid chloride. (a) Totally cross-linked polymer chain, (b) polymer chain with pendant-NH and -COOH, (c) pendant chain with pendant-NH_2 and -NH, and (d) polymer chain with pendant-COOH.

1,3,5-benzenetricarboxylic acid chloride (TMC), and sodium dodecyl sulfate were obtained from Aladdin Chemical Reagent Co., Ltd. The chemical structures of NH_2-BDC, TETA, and TMC are shown in Figure 13. Sodium chloride (NaCl), sodium sulfate (Na_2SO_4), magnesium chloride hexahydrate ($MgCl_2{\cdot}6H_2O$), magnesium sulfate ($MgSO_4$), sodium hydroxide (NaOH), N,N-dimethylformamide (DMF), n-hexane, hydrochloric acid (HCl), methanol

(CH_3OH), acetic acid (CH_3COOH), potassium bromide (KBr), silver nitrate ($AgNO_3$), and sodium borohydride ($NaBH_4$) were purchased from Sinopharm Chemical Reagent Co. Lysozyme and bovine serum protein were purchased from Shanghai Lanji Technology Development Co., Ltd. Beef extract, peptone, was purchased from Beijing Aobaxing Biotechnology Co., Ltd. E. coli was kindly provided from the Department of Biology, East China University of Technology. Bisphenol A was purchased from Sigma-Aldrich, Ltd.

4.2. Preparation of Ag@UiO-66-NH_2 Particles

4.2.1. Synthesis of UiO-66-NH_2. UiO-66-NH_2 nanoparticles were prepared via solvothermal reaction following a procedure reported elsewhere [39]. 0.686 mmol NH_2-BDC was dissolved in 20 mL of DMF/acetic acid mixed solvent (39 : 1). Stoichiometric amount of 0.686 mmol $ZrCl_4$ was then added. Subsequently, the reaction mixture was sonicated for 15 min, added into a 50 mL hydrothermal reactor, and then maintained at 120°C for 24 h. The white solids generated were recovered by centrifuging (5 min, 4000 rpm), washed with DMF for three times. To completely remove the unreacted ligands inside the framework, the solids were soaked in 30 mL DMF and heated at 80°C for 6 h. Then, the DMF trapped in the samples was exchanged by methanol for 3 days at ambient temperature, followed by drying at 120°C in vacuum oven overnight to afford the final products.

4.2.2. Synthesis of Ag^+@UiO-66-NH_2. 3 g UiO-66-NH_2 was added into 50 mL 9 wt% $AgNO_3$ solution, stirred at 60°C for 1 h, and kept in the solution for 24 h; then, the UiO-66-NH_2 particles absorbed Ag^+ were separated from the solution by centrifuging. The excess Ag^+ was washed with deionized water and then vacuum dried at 60°C for 24 h to obtain Ag^+@UiO-66-NH_2 particles.

4.2.3. Synthesis of Ag@UiO-66-NH_2. 3 g Ag^+@UiO-66-NH_2 and 0.09 g $NaHB_4$ were added into 50 mL and 0.01 mol/L NaOH solution. After pH was adjusted to 8, the samples were stirred and reacted for 2 h, centrifuged, washed by deionized water, and dried at 60°C to obtain Ag@UiO-66-NH_2. The schematical illustration of the preparation processes of Ag@UiO-66-NH_2 is shown in Figure 14.

4.3. Fabrication of Ag@UiO-66-NH_2/Polyamide Nanofiltration Membrane. The polyacrylonitrile (PAN) ultrafiltration membrane was immersed into 144 mL 0.6 wt % triethylenetetramine (TETA) solution containing 0.5 wt% sodium dodecyl sulfate for 30 min. The membrane was taken out, dried, and then immersed into 86.4 mL 0.5 wt% of 1,3,5-benzenetricarboxylic acid chloride, and n-hexane solution containing Ag@UiO-66-NH_2 particles ranged from 0 g to 0.05 g for 90 s. The membrane was removed and put into a 60°C oven for 10 min. After cooling, the membrane was stored in deionized water for subsequent structural characterization and performance testing. The membrane fabrication procedure and possible polymerization reaction between triethylenetetramine and 1,3,5-benzenetricarboxylic acid chloride are shown in Figures 15 and 16.

The membranes prepared by incorporating 0 g, 0.01 g, 0.02 g, 0.03 g, 0.04 g, and 0.05 g Ag@UiO-66-NH_2 were named as NF-Ag-0, NF-Ag-1, NF-Ag-2, NF-Ag-3, NF-Ag-4, and NF-Ag-5, respectively.

4.4. Characterization of Ag@UiO-66-NH_2. Chemical composition of UiO-66-NH_2 and Ag@UiO-66-NH_2 was characterized by Nicolet 380 FTIR spectrometer (USA) in the range of 400-4000 cm^{-1}. The crystalline structure of nanoparticles was analyzed by X-ray diffraction (XRD, D8 ADVANCE, Germany) using Cu Ka radiation ($\lambda = 1.54$ Å) at 40 kV and 40 mA in the interval of $5° \le 2\theta \le 80°$. Transmission electron microscopy (TEM, JEL-2100, Japan) at an acceleration voltage of 100 kV was used to determine the size and morphology of UiO-66-NH_2 and Ag@UiO-66-NH_2 nanoparticles. N_2 sorption isotherms of UiO-66-NH_2 and Ag@UiO-66-NH_2 were collected by a Quantachrome Autosorbe-1 analyzer at 77 k, and the surface area of UiO-66-NH_2 and Ag@UiO-66-NH_2 was calculated by Brunauer-Emmer-Teller (BET).

4.5. Characterization of Ag@UiO-66-NH_2/Polyamide Membrane. Chemical composition of the membranes surface was analyzed based on attenuated total reflectance infrared spectroscopy (ATR-FTIR, Nicolet-380 USA) in the range of 400-4000 cm^{-1}. The morphology of the membranes was observed by scanning electron microscopy (SEM, FEI Nova NanoSEM450, Czech Republic) at accelerated voltage of 10 kV. The element distribution on the membrane surface was characterized by energy spectrum analyzer (EDS) attached to SEM.

4.6. Separation Performance of the Membranes. All the separation measurements were carried out in a cross-flow cell with a membrane area of 23.75 cm^2. The membranes were first stabilized for 30 min at 0.8 MPa; then, the rejection rate and flux of 1000 mg/L NaCl, Na_2SO_4, $MgCl_2$, $MgSO_4$, and 5 mg/L to 50 mg/L biphenol A solution were measured at 0.6 MPa at room temperature. All the tests were repeated at least three times to obtain the performance of each fabricated membranes.

The permeance (J, $L{\cdot}m^{-2}{\cdot}h^{-1}$) of the membrane is calculated by Equation (1)

$$J = \frac{V}{A \times t}, \tag{1}$$

where J is the flux ($L{\cdot}m^{-2}{\cdot}h^{-1}$), V is the volume of liquid passing through in t time (L), A is the effective membrane area (m^2), and t is the time (h).

The solute rejection rate of the membrane is calculated by Equation (2)

$$\frac{R}{(\%)} = \left(\frac{C_f - C_p}{C_f}\right) \times 100. \tag{2}$$

R is the rejection rate; C_f is the concentration of the feed

liquid; C_p is the permeation concentration. Salt concentrations of permeate and feed solutions were tested by electrical conductivity (DDS-11A, Shanghai Leici Instrument Co., Shanghai, China). Concentration of biphenol A was measured by UV-visible spectrophotometer (T6, Beijing General Analysis Instrument Co., Ltd.) at 276 nm.

4.7. Hydrophilic Characterization. The hydrophilicity of the membrane surface was characterized by water contact angle measurements (JC2000CI, Shanghai, China) by sessile drop method. A total of 1 μL of deionized water was dropped onto a dry membrane with a microsyringe in an atmosphere of saturated water vapor at room temperature. The size of the drip was captured by video, and the water contact angle was measured by goniometer. At least 5 contact angles were averaged to obtain a reliable value.

4.8. Antifouling Experiments

4.8.1. Antimicrobial Resistance. Using Escherichia coli as model bacteria, the antibacterial properties of nanofiltration membranes were investigated by dilution coating plate method. Escherichia coli was first inoculated in beef extract peptone liquid medium, cultured in a shaking oven at 37°C (150 r/min) for 24 h, and diluted to 10^5 CFU/mL~10^6 CFU/ml for subsequent testing.

1 cm × 2 cm membrane was put into a test tube containing diluted bacterial solution and cultured at 37°C for 24 h, then was taken out, and washed by 15 ml liquid medium. Dilute the flushing solution to a certain concentration; then, take 200 μ L diluted flushing solution evenly coated on beef extract peptone solid medium and cultured at 37°C for 24 h. Count the number of live bacteria and calculate the antibacterial rate by the following equation:

$$\frac{S}{(\%)} = \left(\frac{M-N}{M}\right) \times 100, \tag{3}$$

where M is the number of bacterial colonies of PAN membrane and N is the number of bacterial colonies of typical nanofiltration membrane.

4.8.2. Antiprotein Adsorption. To evaluate antifouling property of the membranes, dynamic filtration experiment was performed with BSA and Lys, respectively. The membranes were precompacted by DI water at 25°C and 0.8 MPa for 30 min until achieving a stable state, and the filtration experiment was cycled.

The pure water permeation flux J_{w0} was measured for 1 h at 0.6 MPa, and model contaminant solution (1000 mg/L BSA or Lys) was filtrated for another 1 h to obtain flux J_{w1}. After which, the filtrated membrane was washed by deionized water for 1 h to remove foulant molecules and water flux J_{w2} was measured. The membrane flux recovery rate (FRR), reversible pollution index (R_r), and irreversible pollution index (R_{ir}) were calculated as follows:

$$\frac{\text{FRR}}{(\%)} = \left(\frac{J_{w2}}{J_{w0}}\right) \times 100, \tag{4}$$

$$\frac{R_r}{(\%)} = \left(\frac{J_{w2}-J_{w1}}{J_{w0}}\right) \times 100, \tag{5}$$

$$\frac{R_{\text{ir}}}{(\%)} = \left(\frac{J_{w0}-J_{w2}}{J_{w0}}\right) \times 100, \tag{6}$$

where J_{W0} is the pure water flux of the membrane, J_{w1} is the BSA or Lys flux of the membrane, and J_{W2} is the pure water flux of the membrane after cleaning.

Data Availability

All data included in this study are available upon request by contacting with the corresponding author.

Conflicts of Interest

The authors declare no conflict of interest.

Acknowledgments

The authors greatly acknowledge the support of the National Natural Science Foundation of China (Nos. 51463001 and 52163027), the opening project of Jiangxi Province Key Laboratory of Polymer Micro/Nano Manufacturing and Devices (PMND201903), the opening fund of State Key Laboratory of Nuclear Resources and Environment (No. NRE1609), the open project program of State Key Laboratory of Petroleum Pollution Control (Grant No. PPC2018008), and the CNPC Research Institute of Safety and Environmental Technology and Foundation of Jiangxi Provincial Department of Education (GJJ190368).

Supplementary Materials

The supplement files include graphical abstract which describes the preparation and performances of Ag@UiO-66-NH_2-modified polyamide nanofiltration membrane. *(Supplementary Materials)*

References

[1] K. Tonova, M. Lazarova, M. Dencheva-Zarkova et al., "Separation of glucose, other reducing sugars and phenolics from natural extract by nanofiltration: Effect of pressure and cross-flow velocity," *Chemical Engineering Research and Design*, vol. 162, p. 107, 2020.

[2] A. Werner, A. Rieger, K. Helbig et al., "Nanofiltration for the recovery of indium and germanium from bioleaching solutions," *Separation and Purification Technology*, vol. 224, p. 543, 2019.

[3] X. S. Zhang, J. Scott, B. K. Sharma, and N. Rajagopalan, "Fouling mitigation and carbon recovery in nanofiltration processing of hydrothermal liquefaction aqueous waste stream," *Journal of Membrane Science*, vol. 614, article 118558, 2020.

[4] R. P. Pandey, P. Abdul Rasheed, T. Gomez, R. S. Azam, and K. A. Mahmoud, "A fouling-resistant mixed-matrix nanofiltration membrane based on covalently cross-linked Ti3C2TX (MXene)/cellulose acetate," *Journal of Membrane Science*, vol. 607, article 118139, 2020.

[5] A. Venault, M. R. B. Ballad, Y. T. Huang, Y. H. Liu, C. H. Kao, and Y. Chang, "Antifouling PVDF membrane prepared by VIPS for microalgae harvesting," *Chemical Engineering Science*, vol. 142, pp. 97–111, 2016.

[6] B. P. Tripathi, P. Das, F. Simon, and M. Stamm, "Ultralow fouling membranes by surface modification with functional polydopamine," *European Polymer Journal*, vol. 99, p. 80, 2018.

[7] N. G. P. Chew, S. S. Zhao, C. Malde, and R. Wang, "Superoleophobic surface modification for robust membrane distillation performance," *Journal of Membrane Science*, vol. 541, p. 162, 2017.

[8] V. Kochkodan, D. J. Johnson, and N. Hilal, "Polymeric membranes: Surface modification for minimizing (bio) colloidal fouling," *Advances in Colloid and Interface Science*, vol. 206, pp. 116–140, 2014.

[9] Y. Zhang, Y. Wan, G. Y. Pan et al., "Surface modification of polyamide reverse osmosis membrane with organic-inorganic hybrid material for antifouling," *Applied Surface Science*, vol. 433, pp. 139–148, 2018.

[10] S. M. Hosseini, M. Afshari, A. R. Fazlali et al., "Mixed matrix PES-based nanofiltration membrane decorated by (Fe_3O_4–polyvinylpyrrolidone) composite nanoparticles with intensified antifouling and separation characteristics," *Chemical Engineering Research and Design*, vol. 147, pp. 390–398, 2019.

[11] R. M. Gol, A. Bera, S. Banjo, B. Ganguly, and S. K. Jewrajka, "Effect of amine spacer of PEG on the properties, performance and antifouling behavior of poly(piperazineamide) thin film composite nanofiltration membranes prepared by *in situ* PEGylation approach," *Journal of Membrane Science*, vol. 472, pp. 154–166, 2014.

[12] M. B. He, T. Li, M. L. Hu et al., "Performance improvement for thin-film composite nanofiltration membranes prepared on PSf/PSf-g-PEG blended substrates," *Separation and Purification Technology*, vol. 230, article 115855, 2020.

[13] E. Bagheripour, A. R. Moghadassi, F. Parvizian, S. M. Hosseini, and B. Van der Bruggen, "Tailoring the separation performance and fouling reduction of PES based nanofiltration membrane by using a PVA/Fe_3O_4 coating layer," *Chemical Engineering Research and Design*, vol. 144, pp. 418–428, 2019.

[14] J. D. Wu, C. Zhang, S. T. Xu, X. Y. Pang, G. Q. Caia, and J. P. Wang, "Preparation of Zwitterionic Polymer-Functionalized Cotton Fabrics and the Performance of Anti-Biofouling and Long-Term Biofilm Resistance," *Colloid and Interface Science Communications*, vol. 24, pp. 98–104, 2018.

[15] M. M. Zhu, Y. Fang, Y. C. Chen et al., "Antifouling and antibacterial behavior of membranes containing quaternary ammonium and zwitterionic polymers," *Journal of Colloid and Interface Science*, vol. 584, pp. 225–235, 2021.

[16] Q. Y. Bi, C. Zhang, J. D. Liu, X. L. Liu, and S. A. Xu, "Positively charged zwitterion-carbon nitride functionalized nanofiltration membranes with excellent separation performance of Mg_{2+}/Li_{+} and good antifouling properties," *Separation and Purification Technology*, vol. 257, article 117959, 2021.

[17] L. Y. Deng, S. L. Li, Y. W. Qin et al., "Fabrication of antifouling thin-film composite nanofiltration membrane via surface grafting of polyethyleneimine followed by zwitterionic modification," *Journal of Membrane Science*, vol. 619, article 118564, 2021.

[18] J. Wang, Z. Wang, Y. Y. Liu, J. X. Wang, and S. C. Wang, "Surface modification of NF membrane with zwitterionic polymer to improve anti-biofouling property," *Journal of Membrane Science*, vol. 514, pp. 407–417, 2016.

[19] V. Vatanpour, S. S. Madaeni, R. Moradian, S. Zinadini, and B. Astinchap, "Novel antibifouling nanofiltration polyethersulfone membrane fabricated from embedding TiO2 coated multiwalled carbon nanotubes," *Separation and Purification Technology*, vol. 90, pp. 69–82, 2012.

[20] R. B. Soria, J. Y. Zhu, I. Gonza, B. Van der Bruggen, and P. Luis, "Effect of (TiO_2: ZnO) ratio on the anti-fouling properties of bio-inspired nanofiltration membranes," *Separation and Purification Technology*, vol. 251, article 117280, 2020.

[21] N. H. H. Hairom, A. W. Mohammad, and A. A. H. Kadhum, "Influence of zinc oxide nanoparticles in the nanofiltration of hazardous Congo red dyes," *Chemical Engineering Journal*, vol. 260, pp. 907–915, 2015.

[22] A. A. Alshahrani, I. H. Alsohaimi, S. Alshehri et al., "Nanofiltration membranes prepared from pristine and functionalised multiwall carbon nanotubes/biopolymer composites for water treatment applications," *Journal of Materials Research and Technology*, vol. 9, no. 4, pp. 9080–9092, 2020.

[23] Y. T. Zhang, Q. Q. Song, X. Liang, J. Wang, Y. L. Jiang, and J. D. Liu, "High-flux, high-selectivity loose nanofiltration membrane mixed with zwitterionic functionalized silica for dye/salt separation," *Applied Surface Science*, vol. 515, article 146005, 2020.

[24] G. Em, C. P. Romanos, F. K. Athanasekou et al., "Double-side active TiO2-modified nanofiltration membranes in continuous flow photocatalytic reactors for effective water purification," *Journal of Hazardous Materials*, vol. 211–212, pp. 304–316, 2012.

[25] Y. C. Liu, Z. X. Yu, Y. X. Peng, L. Y. Shao, X. H. Li, and H. J. Zeng, "A novel photocatalytic self-cleaning TiO_2 nanorods inserted graphene oxide-based nanofiltration membrane," *Chemical Physics Letters*, vol. 749, article 137424, 2020.

[26] X. L. Wang, W. Qin, L. X. Wang et al., "Desalination of dye utilizing carboxylated TiO_2/calcium alginate hydrogel nanofiltration membrane with high salt permeation," *Separation and Purification Technology*, vol. 253, article 117475, 2020.

[27] Y. S. Meng, L. Shu, L. Liu et al., "A high-flux mixed matrix nanofiltration membrane with highly water-dispersible MOF crystallites as filler," *Journal of Membrane Science*, vol. 591, article 117360, 2019.

[28] N. Misdan, N. Ramlee, N. H. H. Hairom et al., "CuBTC metal organic framework incorporation for enhancing separation and antifouling properties of nanofiltration membrane," *Chemical Engineering Research and Design*, vol. 148, pp. 227–239, 2019.

[29] P. Zhang, J. L. Gong, G. M. Zeng et al., "Ultrathin reduced graphene oxide/MOF nanofiltration membrane with improved purification performance at low pressure," *Chemosphere*, vol. 204, pp. 378–389, 2018.

[30] S. Fatemeh Seyedpour, A. Rahimpour, and G. Najafpour, "Facile in-situ assembly of silver-based MOFs to surface functionalization of TFC membrane: A novel approach toward long-lasting biofouling mitigation," *Journal of Membrane Science*, vol. 573, pp. 257–269, 2019.

[31] M. Pejman, M. D. Firouzjaei, S. A. Aktij et al., "Improved antifouling and antibacterial properties of forward osmosis membranes through surface modification with zwitterions and silver-based metal organic frameworks," *Journal of Membrane Science*, vol. 611, article 118352, 2020.

[32] M. Pejman, M. D. Firouzjaei, S. A. Aktij et al., "Effective strategy for UV-mediated grafting of biocidal Ag-MOFs on polymeric membranes aimed at enhanced water ultrafiltration," *Chemical Engineering Journal*, vol. 426, article 130704, 2021.

[33] A. Gupta, L. T. Phung, and S. Silver, "Diversity of silver resistance genes in IncH incompatibility group plasmids," *Microbiology*, vol. 147, p. 3393, 2001.

[34] Z. M. Liu, J. E. Stout, M. Boldin, J. Rugh, W. F. Diven, and V. L. Yu, "Intermittent Use of Copper-Silver Ionization for *Legionella* Control in Water Distribution Systems: A Potential Option in Buildings Housing Individuals at Low Risk of Infection," *Clinical Infectious Diseases*, vol. 26, pp. 138–140, 1998.

[35] A. Q. Shi, C. S. Zhu, S. Fu et al., "What controls the antibacterial activity of Ti-Ag alloy, Ag ion or Ti2Ag particles?," *Materials Science and Engineering: C*, vol. 109, article 110548, 2020.

[36] Y. Liu, P. Cheng, Q. H. Guo et al., "Ag nanoparticles decorated PVA-*co*-PE nanofibrous microfiltration membrane with antifouling surface for efficient sterilization," *Composites Communications*, vol. 21, article 100379, 2020.

[37] N. Haghighat, V. Vatanpour, M. Sheydaei, and Z. Nikjavan, "Preparation of a novel polyvinyl chloride (PVC) ultrafiltration membrane modified with Ag/TiO2 nanoparticle with enhanced hydrophilicity and antibacterial activities," *Separation and Purification Technology*, vol. 237, article 116374, 2020.

[38] A. Yildiz, D. V. Bayramol, R. Atav et al., "Synthesis and characterization of Fe_3O_4@ Cs@ Ag nanocomposite and its use in the production of magnetic and antibacterial nanofibrous membranes," *Surface Science*, vol. 541, article 146332, 2020.

[39] L. Ding, P. H. Shao, Y. Luo et al., "Functionalization of UiO-66-NH_2 with rhodanine via amidation: Towarding a robust adsorbent with dual coordination sites for selective capture of Ag(I) from wastewater," *Chemical Engineering Journal*, vol. 382, article 123009, 2020.

[40] Y. M. Xu, S. Japip, and T. S. Chung, "Mixed matrix membranes with nano-sized functional UiO-66-type MOFs embedded in 6FDA-HAB/DABA polyimide for dehydration of C1-C3 alcohols via pervaporation," *Journal of Membrane Science*, vol. 549, pp. 217–226, 2018.

[41] L. H. Ni, Z. P. Liao, K. Chen et al., "Defect-engineered UiO-66-NH2 modified thin film nanocomposite membrane with enhanced nanofiltration performance," *Chemical Communications*, vol. 56, no. 60, p. 8372, 2020.

[42] L. Cseri, R. Hardian, S. Anan et al., "Bridging the interfacial gap in mixed-matrix membranes by nature-inspired design: Precise molecular sieving with polymer-grafted metal–organic frameworks," *Journal of Materials Chemistry A*, vol. 9, article 23793, 2021.

[43] X. Zhang, Y. F. Zhang, T. C. Wang, Z. Fan, and G. L. Zhang, "A thin film nanocomposite membrane with pre-immobilized UiO-66-NH 2 toward enhanced nanofiltration performance," *RSC Advances*, vol. 9, pp. 24802–24810, 2019.

[44] Z. F. Gao, Y. N. Feng, D. C. Ma, and T. S. Chung, "Vapor-phase crosslinked mixed matrix membranes with UiO-66-NH2 for organic solvent nanofiltration," *Journal of Membrane Science*, vol. 574, pp. 124–135, 2019.

[45] J. J. Sun, S. Feng, and S. S. Feng, "Hydrothermally synthesis of MWCNT/N-TiO2/UiO-66-NH2 ternary composite with enhanced photocatalytic performance for ketoprofen," *Inorganic Chemistry Communications*, vol. 111, Article ID 107669, 2020.

[46] X. Li, Y. L. Xu, K. L. Goh, T. H. Chong, and R. Wang, "Layer-by-layer assembly based low pressure biocatalytic nanofiltration membranes for micropollutants removal," *Journal of Membrane Science*, vol. 615, article 118514, 2020.

[47] S. Yüksel, N. Kabay, and M. Yüksel, "Removal of bisphenol A (BPA) from water by various nanofiltration (NF) and reverse osmosis (RO) membranes," *Journal of Hazardous Materials*, vol. 263, pp. 307–310, 2013.

[48] I. Escalona, A. Fortuny, F. Stüber, C. Bengoa, A. Fabregat, and J. Font, "Fenton coupled with nanofiltration for elimination of bisphenol A," *Desalination*, vol. 345, pp. 77–84, 2014.

[49] K. Kimura, S. Toshima, G. Amy, and Y. Watanabe, "Rejection of neutral endocrine disrupting compounds (EDCs) and pharmaceutical active compounds (PhACs) by RO membranes," *Journal of Membrane Science*, vol. 245, pp. 71–78, 2004.

[50] N. Bolong, A. F. Ismail, M. R. Salim, D. Rana, T. Matsuura, and A. Tabe-Mohammadi, "Negatively charged polyethersulfone hollow fiber nanofiltration membrane for the removal of bisphenol A from wastewater," *Separation and Purification Technology*, vol. 73, no. 2, pp. 92–99, 2010.

[51] A. M. Comerton, R. C. Andrews, D. M. Bagley, and C. Y. Hao, "The rejection of endocrine disrupting and pharmaceutically active compounds by NF and RO membranes as a function of compound and water matrix properties," *Journal of Membrane Science*, vol. 313, pp. 323–335, 2008.

[52] A. M. Zahari, C. W. Shuo, P. Sathishkumar et al., "A reusable electrospun PVDF-PVP-MnO_2 nanocomposite membrane for bisphenol A removal from drinking water," *Chemical Engineer*, vol. 6, pp. 5801–5811, 2018.

[53] A. Kubiak, M. Maćkiewicz, M. Biesaga, and M. Karbarz, "Highly efficient removal of bisphenols from aqueous solution using environmental-sensitive microgel," *Journal of Environmental Chemical Engineering*, vol. 9, article 104947, 2021.